

Disappearance of N_2H^+ from the gas phase in the class 0 protostar IRAM 04191^{*}

A. Belloche^{1,2} and P. André³

¹ Max-Planck-Institut für Radioastronomie, Auf dem Hügel 69, 53121 Bonn, Germany

² LERMA/LRA, École Normale Supérieure, 24 rue Lhomond, 75231 Paris Cedex 05, France

³ Service d'Astrophysique, CEA/DSM/DAPNIA, C.E. Saclay, 91191 Gif-sur-Yvette Cedex, France
e-mail: pandre@cea.fr

Received 23 February 2004 / Accepted 10 April 2004

Abstract. We present a high-resolution millimeter study of the very young class 0 protostar IRAM 04191+1522 in the Taurus molecular cloud. $N_2H^+(1-0)$ observations with the IRAM Plateau de Bure Interferometer and 30 m telescope demonstrate that the molecular ion N_2H^+ disappears from the gas phase in the inner part of the protostellar envelope ($r < 1600$ AU, $n_{H_2} > 5 \times 10^5$ cm⁻³). This result departs from the predictions of current chemical models. It suggests either that N_2 is more depleted than the models predict, owing to a higher binding energy on polar ice or an enhanced grain chemistry transforming N_2 to less volatile species, or that strong deuterium fractionation enhances N_2D^+ to the detriment of N_2H^+ .

Key words. stars: formation – circumstellar matter – stars: individual: IRAM 04191+1522 – ISM: abundances – astrochemistry – stars: rotation

1. Introduction

Understanding the onset of gravitational collapse in dense cloud cores requires detailed (sub)millimeter studies of the structure of prestellar condensations and young protostars (e.g., André et al. 2000). However, recent observations have shown that molecules such as CO and CS deplete onto grain surfaces in the inner parts of dense cores (e.g., Bacmann et al. 2002; Tafalla et al. 2002). Since this depletion phenomenon is thought to affect many other species at high densities, studying the kinematics of pre/protostellar cores with future high-resolution instruments such as ALMA may be difficult and requires the identification of the best tracers of dense gas. N_2H^+ has been put forward as such a good tracer since it is much less sensitive to depletion effects than other species observed with single-dish telescopes (e.g., Tafalla et al. 2002), even though Bergin et al. (2002) reported a slight decrease of its abundance toward the prestellar core B68.

Prime targets for observational studies of protostellar collapse are very young class 0 objects such as IRAM 04191+1522 – hereafter IRAM 04191 for short – in Taurus (see André et al. 1999 – hereafter AMB99). This protostar features a prominent (~ 0.5 – $1.5 M_\odot$) envelope and a powerful bipolar outflow, but lacks a sizeable accretion disk.

Send offprint requests to: A. Belloche,
e-mail: belloche@mpi.fr-bonn.mpg.de

^{*} Based on observations carried out with the IRAM Plateau de Bure Interferometer. IRAM is supported by INSU/CNRS (France), MPG (Germany) and IGN (Spain).

Belloche et al. (2002 – hereafter BADB02) showed that the envelope is undergoing both extended infall motions and fast, differential rotation. They proposed that the rapidly rotating inner envelope ($r < 3500$ AU) corresponds to a magnetically supercritical core decoupling from an environment still supported by magnetic fields and strongly affected by magnetic braking.

Here, we report new observations of IRAM 04191 carried out with the Plateau de Bure interferometer (PdBI) in the $N_2H^+(1-0)$ line in an effort to probe the inner structure of the envelope. We discuss the results of these high-resolution observations which show that N_2H^+ disappears from the gas phase in the inner part of the envelope.

2. Observations and data reduction

We observed IRAM 04191 with the PdBI for 34 h between December 2001 and September 2002 with 4 to 6 antennas in the C and D configurations. In the 3 mm band, each receiver was tuned to the $N_2H^+(101-012)$ line at 93.176258 GHz in single side-band mode. The system temperatures were typically 110–200 K. The 39 kHz channel spacing resulted in a velocity resolution of 0.20 km s⁻¹ (see Wiesemeyer 2001). The (naturally-weighted) synthesized half-power beam width was 5.8'' \times 4.0'' (810 AU \times 560 AU) and the (*FWHM*) primary beam $\sim 54''$. Several nearby phase calibrators were observed to determine the time-dependent complex antenna gains. The correlator bandpass was calibrated on the sources 3C 84, 0415+379, 3C 273, 3C 454.3 or NRAO 150, while the absolute flux density scale was derived from MWC 349 or 3C 84.

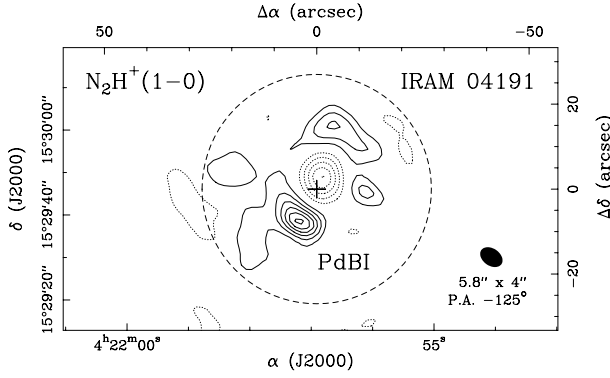


Fig. 1. $\text{N}_2\text{H}^+(1-0)$ integrated intensity map of the IRAM 04191 inner envelope obtained with PdBI (uncorrected for primary beam attenuation). The emission is integrated over three velocity intervals covering the whole seven-component multiplet. The contours vary from -0.5 to -0.1 (dotted contours) and from 0.1 to 0.6 (solid contours), by step of $0.1 \text{ Jy beam}^{-1} \text{ km s}^{-1}$ (i.e. 3 times the rms noise level). The $54''$ ($FWHM$) primary beam is shown as a big circle and the synthesized clean beam (HPBW) is in the bottom right corner. The cross marks the central 1.3 mm continuum position of IRAM 04191 (cf. BADB02).

The absolute calibration uncertainty is estimated to be $\sim 15\%$. The data were calibrated and imaged using the GILDAS software (Jan. 2002 release). The deconvolution was performed with the CLEAN method, down to 0.6 times the rms noise level.

The present study also uses single-dish $\text{N}_2\text{H}^+(1-0)$ and 1.3 mm continuum on-the-fly maps taken with the IRAM 30 m telescope (see BADB02 and Motte & André 2001 – hereafter MA01), as well as 1.3 mm continuum interferometric data obtained with PdBI in 1999 (see BADB02). The combination of the PdBI and single-dish data was performed in the uv -plane (see Guilloteau 2001). We used a single-dish calibration factor of $5.9 \text{ Jy beam}^{-1} \text{ K}^{-1}$ for $\text{N}_2\text{H}^+(1-0)$ (Greve et al. 1998). For the continuum data, we applied a calibration factor of 1.35 to account for the difference in observed frequency (227 GHz at PdBI and $\sim 250 \text{ GHz}$ for bolometer observations at the 30 m).

3. Analysis: A drop in N_2H^+ abundance

3.1. A central hole of N_2H^+ emission

The $\text{N}_2\text{H}^+(1-0)$ integrated intensity map obtained with PdBI shows two emission peaks to the South-East and North-West of the central IRAM 04191 position (see Fig. 1). An emission gap with negative contours down to the -15σ level is also seen close to the central position, shifted by $3.5''$ (i.e., less than one beam width) to the North-West. These three features, which form a structure elongated roughly perpendicular to the outflow axis, have the same relative intensities in each ΔF_1 group of hyperfine components of the $\text{N}_2\text{H}^+(1-0)$ multiplet. To recover the extended emission filtered out by the interferometer and obtain reliable N_2H^+ column densities, we combined our PdBI observations with short-spacing data obtained with the 30 m telescope (BADB02). The resulting map of $\text{N}_2\text{H}^+(1-0)$ integrated intensity reveals a ring-shaped core with two local peaks, surrounding an emission gap near the center (see Fig. 2).

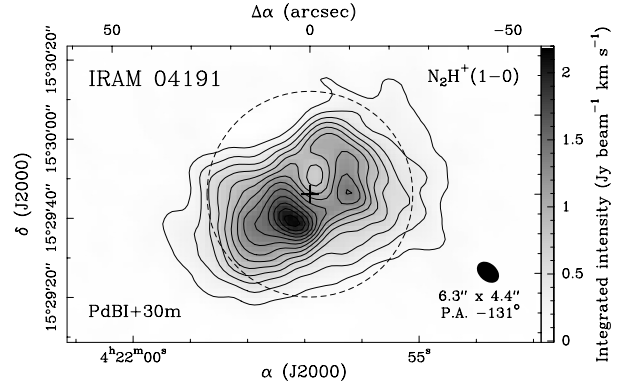


Fig. 2. $\text{N}_2\text{H}^+(1-0)$ integrated intensity map of the IRAM 04191 envelope combining PdBI and 30 m data. The emission is integrated over the same velocity intervals as in Fig. 1. The contours vary from 0.16 to 2.1 by step of $0.16 \text{ Jy beam}^{-1} \text{ km s}^{-1}$ (i.e. 6 times the rms noise). The map is *not* corrected for primary beam attenuation (automatically applied to the single-dish data in the combination process); the big circle represents the $FWHM$ primary beam of the PdBI at 3 mm. The synthesized clean beam (HPBW) is shown in the bottom right corner. The cross marks the central position of IRAM 04191.

This gap is a factor of 3.5 (2.3) weaker than the primary (secondary) emission peak to the South-East (West). The detection of such a gap strongly suggests that the N_2H^+ abundance decreases toward the center.

3.2. Optical depths and excitation temperatures

We used the hyperfine structure fitting method of the CLASS software to estimate the optical depths and excitation temperatures of $\text{N}_2\text{H}^+(1-0)$ in the PdBI-30 m combined map. The fits were limited to the spectra with a signal-to-noise ratio larger than 10. We fitted only the 4 ($\Delta F_1 = \pm 1$) components to avoid convergence problems that occurred for a few positions in the western part of the envelope, and may be related to excitation anomalies (e.g., Turner 2001) and/or low signal-to-noise ratio for the weakest (110–011) component. The $1-\sigma$ optical depth uncertainty given by the fits is typically 15–25% for spectra with opacities larger than 5, and 50–150% for optically-thinner spectra. Except for a few positions at $\sim (0'', 15'')$, the total $\text{N}_2\text{H}^+(1-0)$ optical depths are lower than 15, and even lower than 10 toward the brightest emission peak and the emission gap, corresponding to optical depths lower than 1.7 and 1.1, respectively, for the isolated (101–012) component. The excitation temperature was found to vary from 4 K to 10 K across the PdBI-30 m combined map and to display a maximum toward the brightest emission peak of the integrated intensity map.

3.3. Comparison with the dust emission maps

Figure 3 shows the ratio of $\text{N}_2\text{H}^+(101-012)$ integrated intensity to 1.3 mm continuum intensity across the IRAM 04191 envelope. The large greyscale map was obtained using the single-dish 1.3 mm data of MA01 smoothed to the $26.4''$ ($FWHM$) resolution of the 30 m telescope at the $\text{N}_2\text{H}^+(1-0)$ frequency. The ratio was computed only

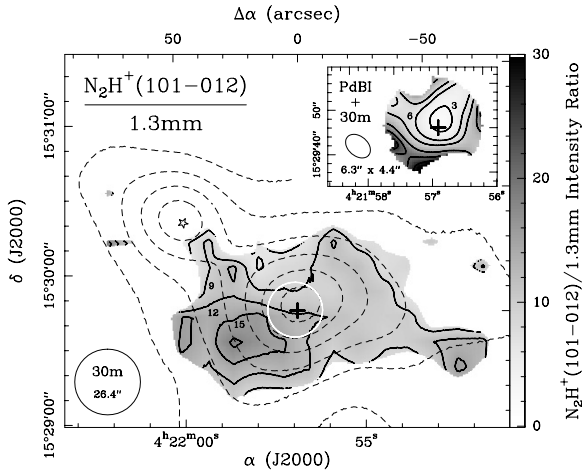


Fig. 3. Greyscale map of the ratio of $N_2H^+(101-012)$ integrated intensity to 1.3 mm continuum intensity, both observed with the 30 m telescope. The (thick) contours go from 6 to 18 by 3 $Jy beam^{-1} km s^{-1}/(Jy beam^{-1})$. The 1.3 mm continuum map smoothed to the $N_2H^+(1-0)$ resolution is overlaid as dashed contours. The insert in the top-right corner shows the PdBI-30 m combined map of the same ratio, limited to the 22'' PdBI primary beam at 227 GHz (corresponding to the white circle in the larger map). The greyscale is the same as for the larger map; the contours go from 3 to 9 by 3 and from 15 to 27 by 6 $Jy beam^{-1} km s^{-1}/(Jy beam^{-1})$. The beam sizes are shown in both maps. The cross marks the position of IRAM 04191, the star indicates the position of the class I object IRAS 04191.

at positions where both the 1.3 mm and $N_2H^+(101-012)$ intensities were stronger than 4 times the rms noise. The higher-resolution, smaller greyscale map in the insert of Fig. 3 displays the same $N_2H^+(101-012)$ to dust continuum ratio derived from the PdBI-30 m combined data for both the $N_2H^+(101-012)$ and 1.3 mm continuum emission. The PdBI continuum data were recalibrated to the frequency of the 30 m continuum data prior to combination (see Sect. 2), and the 1.3 mm combined map was smoothed to the resolution of the $N_2H^+(1-0)$ combined map. The ratio of the two sets of combined data was computed after correction for the respective PdBI primary beam attenuations at 3 mm and 1.3 mm.

The $N_2H^+(1-0)$ integrated intensity is expected to primarily track the variations of N_2H^+ column density (see Fig. 4a). Indeed, $N_2H^+(1-0)$ is thermalized for $n_{H_2} > 10^5 cm^{-3}$, and the gas/dust temperatures (which are well coupled above this density – Doty & Neufeld 1997) are in the range 6.5–10 K (cf. Fig. 7d of BADB02), i.e., in a regime where the LTE line intensities depend only weakly on temperature. The 1.3 mm continuum intensity, on the other hand, should scale as the H_2 column density times the dust temperature times the dust opacity (see, e.g., Eq. (1) of Motte et al. 1998). The bolometric luminosity of IRAM 04191 is so low ($L_{bol} \sim 0.15 L_{\odot}$ – see AMB99) that the dust temperature is expected to vary by less than 50% in the range of radii 400–2800 AU (see BADB02). The variations of the intensity ratio in the central $r < 2800$ AU ($r_{\theta} < 20''$) region around IRAM 04191 should thus reflect the variations of the N_2H^+ abundance, to within a factor of ~ 2 if we account for a possible slight saturation of $N_2H^+(101-012)$ ($\tau_{101-012} < 1.7$, see Sect. 3.2) and possible changes in the dust opacity.

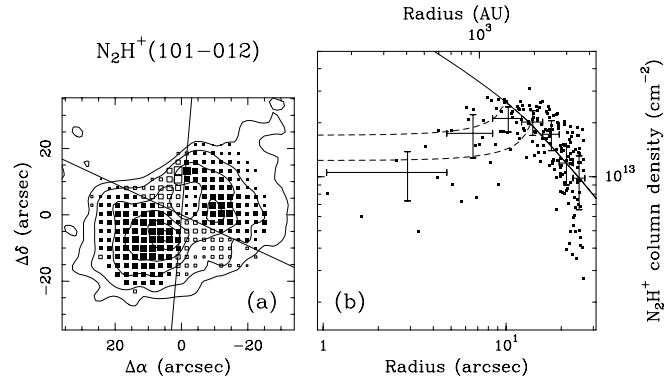


Fig. 4. **a)** Map of the N_2H^+ column density $N_{N_2H^+}$ (squares) derived from the $N_2H^+(101-012)$ integrated intensity map overlaid as contours (0.03, 0.06 to 0.3 by step of 0.06 $Jy beam^{-1} km s^{-1}$). The size of each square increases linearly with $N_{N_2H^+}$, from 2.6×10^{12} to $3.3 \times 10^{13} cm^{-2}$. **b)** Circularly-averaged radial profile of $N_{N_2H^+}$. The crosses with error bars represent the average $N_{N_2H^+}$ in concentric annuli limited to the positions shown with filled squares in **a)**. The solid curve shows the H_2 column density profile (MA01) scaled to the 7th annulus for comparison. The two dashed curves illustrate the effect of a central hole of N_2H^+ material of radius 1350 AU and 1850 AU, respectively.

The intensity ratio has an average value of $\sim 11 Jy beam^{-1} km s^{-1}/(Jy beam^{-1})$ in the central ($r_{\theta} < 20''$) region of the single-dish map, and drops to a minimum of $2.7 Jy beam^{-1} km s^{-1}/(Jy beam^{-1})$ near the center of the high-resolution map. We conclude that the N_2H^+ abundance averaged along the line of sight decreases by a factor of ~ 4 from $r_{\theta} \sim 20''$ to $r_{\theta} \sim 5''$.

3.4. Disappearance of N_2H^+ from the gas phase

The map of N_2H^+ column density shown in Fig. 4a was computed using a LTE partition function at the $N_2H^+(1-0)$ excitation temperature derived from the hfs fits, assumed to be uniform along each line of sight. We also applied an optical depth correction of $\tau/(1 - e^{-\tau})$ using the hfs fit results. Figure 4b compares the circularly-averaged radial profile of N_2H^+ column density with the H_2 column density profile derived from the dust emission (MA01). The former clearly departs from the latter for $\theta \leq 13''$. A good model fit is obtained when one assumes a hole of N_2H^+ material in the central part of the envelope ($r < 1350-1850$ AU, see dashed curves). This comparison strongly suggests that the N_2H^+ ion disappears from the gas phase above a density of $n_{H_2} \sim 4-7 \times 10^5 cm^{-3}$ in the IRAM 04191 envelope, according to the density profile derived by MA01 (see Fig. 7a of BADB02). We derive a mean N_2H^+ abundance of $\sim 7 \pm 4 \times 10^{-10}$ at $r = 3500$ AU.

3.5. Fast, differential rotation

We measure a large velocity difference of $0.47 \pm 0.05 km s^{-1}$ between the two $N_2H^+(1-0)$ emission peaks of the PdBI map shown in Fig. 1, largely exceeding the $FWHM$ linewidths measured toward the peaks themselves ($0.34 \pm 0.08 km s^{-1}$). A least-square linear fit to the LSR-velocity map of the

PdBI-30 m combined data yields a mean velocity gradient of $\sim 17 \text{ km s}^{-1} \text{ pc}^{-1}$ with a position angle of $PA \sim 133^\circ$. This small-scale gradient has a direction consistent with the direction of the mean velocity gradient measured on larger scale with the 30 m telescope by BADB02, but is 5 times larger. The PdBI results thus confirm and strengthen the presence of fast, differential rotation identified by BADB02. The detailed form of the rotation velocity profile, which is confirmed to have a break at $r \lesssim 3000 \text{ AU}$ (see Fig. 12 of BADB02), will be discussed in a forthcoming paper based on radiative transfer simulations taking the N_2H^+ depletion into account.

4. Implications

We showed in Sect. 3.4 that the molecular ion N_2H^+ disappears from the gas phase above a density of $n_{H_2} \sim 5 \times 10^5 \text{ cm}^{-3}$ in the envelope of the class 0 protostar IRAM 04191. This conclusion is at variance with the results of recent chemical models (e.g., Shematovich et al. 2003; Aikawa et al. 2003). In particular, the models calculated by Aikawa et al. (2003) including gas-phase reactions, gas-dust interactions, and diffusive grain-surface reactions predict an *increase* in the N_2H^+ abundance during the prestellar collapse phase up to a density of $n_{H_2} \sim 1 \times 10^7 \text{ cm}^{-3}$ or more. IRAM 04191 is so young, probably less than $3 \times 10^4 \text{ yr}$ since the formation of the central object (AMB99), that it is difficult to invoke a large decrease in the N_2H^+ abundance on such a short timescale at the beginning of the main accretion phase.

Since CO is one of the main destroyers of N_2H^+ in the gas phase (e.g., Aikawa et al. 2001), its potential desorption from grain mantles due to heating by the central protostar could be a mechanism responsible for the disappearance of N_2H^+ from the gas phase. However, the luminosity of IRAM 04191 is so low (see Sect. 3.3) that it is insufficient to raise the dust temperature above 11 K for $r > 400 \text{ AU}$ (J. Bouwman 2003, private communication). Comparing the $C^{18}O(2-1)$ data of BADB02 with the 1.3 mm continuum map of MA01, we measure a reduction of the $C^{18}O$ abundance (averaged along the line of sight) by a factor of ~ 3.5 toward the center of the envelope, assuming an optically thin $C^{18}O$ line¹. There is thus no evidence for any $C^{18}O$ (and thus CO) desorption from the dust grains in the inner envelope at the 30 m resolution (800 AU in radius). This indicates that potential CO desorption due to shocks produced by the outflow does not dominate in the central beam. Although the overall morphology seen in Figs. 2 and 4a suggests that the N_2H^+ abundance may reach a minimum along the outflow path, the outflow is sufficiently well collimated (cf. Fig. 1 of AMB99) that its effect should be negligible in the equatorial plane of the envelope.

We suggest two other possible explanations for the disappearance of N_2H^+ in the IRAM 04191 envelope:

- 1) N_2 may condense onto the grain surfaces. This could be either due to a higher N_2 binding energy on polar ice mantles than the value of 750 K usually adopted (see model C of Aikawa et al. 2001; Bergin et al. 2002), or to an enhanced grain chemistry transforming N_2 into less

volatile species (Aikawa 2003, private communication). Such a strong N_2 depletion was suggested by Caselli et al. (2003) to account for the high H_2D^+ abundance measured in L1544.

- 2) Deuterium fractionation may enhance N_2D^+ over N_2H^+ . A high-degree of deuterium fractionation has indeed been observed in dense cores (e.g., Turner 2001; Bacmann et al. 2003), and Roberts et al. (2003) predict that the N_2D^+/N_2H^+ abundance ratio should even exceed 1 at densities of $\sim 10^6 \text{ cm}^{-3}$ when they include HD_2^+ and D_3^+ in their chemical model. N_2D^+ may thus be a better tracer of dense gas than N_2H^+ .

The disappearance of N_2H^+ from the gas phase suggests that all species bearing heavy elements also vanish at high density in prestellar cores. However, Walmsley et al. (2004) find that, under such conditions, the ionization degree of the gas is not significantly changed owing to the enhanced abundances of H^+ , H_3^+ , and D_3^+ . Moreover, they argue that the ambipolar diffusion timescale is dominated by the coupling of the neutrals to the charged grains at these densities. The dynamics of protostellar collapse may thus be essentially unaffected by the strong molecular depletion in prestellar cores.

Acknowledgements. We would like to thank Y. Aikawa, M. Gerin, G. Pineau des Forêts and M. Walmsley for enlightening discussions about the chemistry. We are grateful to F. Gueth, J. Pety and R. Neri (IRAM) for their help with the Plateau de Bure observations. We would also like to thank F. Motte for her advice about the continuum data.

References

- Aikawa, Y., Ohashi, N., Inutsuka, S. I., Herbst, E., & Takakuwa, S. 2001, *ApJ*, 552, 639
- Aikawa, Y., Ohashi, N., & Herbst, E. 2003, *ApJ*, 593, 906
- André, P., Motte, F., & Bacmann, A. 1999, *ApJ*, 513, L57 (AMB99)
- André, P., Ward-Thompson, D., & Barsony, M. 2000, in *Protostars and Planets IV*, ed. V. Mannings, A. P. Boss, & S. S. Russell (Tucson: Univ. of Arizona Press), 59
- Bacmann, A., Lefloch, B., Ceccarelli, C., et al. 2002, *A&A*, 389, L6
- Bacmann, A., Lefloch, B., Ceccarelli, C., et al. 2003, *ApJ*, 585, L55
- Belloche, A., André, P., Despois, D., & Blinder, S. 2002, *A&A*, 393, 927 (BADB02)
- Bergin, E. A., Alves, J., Huard, T., & Lada, C. J. 2002, *ApJ*, 570, L101
- Caselli, P., van der Tak, F. F. S., Ceccarelli, C., & Bacmann, A. 2003, *A&A*, 403, L37
- Doty, S. D., & Neufeld, D. A. 1997, *ApJ*, 489, 122
- Greve, A., Kramer, C., & Wild, W. 1998, *A&AS*, 133, 271
- Guilloteau, S. 2001, in *Proceedings from the IRAM Millimeter Summer School 2*, ed. A. Dutrey, 219
- Motte, F., & André, P. 2001, *A&A*, 365, 440 (MA01)
- Motte, F., André, P., & Neri, R. 1998, *A&A*, 336, 150
- Roberts, H., Herbst, E., & Millar, T. J. 2003, *ApJ*, 591, L41
- Shematovich, V. I., Wiebe, D. S., Shustov, B. M., & Li, Z. Y. 2003, *ApJ*, 588, 894
- Tafalla, M., Myers, P. C., Caselli, P., Walmsley, C. M., & Comito, C. 2002, *ApJ*, 569, 815
- Turner, B. E. 2001, *ApJS*, 136, 579
- Walmsley, C. M., Flower, D. R., & Pineau des Forêts, G. 2004, *A&A*, in press [arXiv:astro-ph/0402493]
- Wiesemeyer, H. 2001, in *Proceedings from the IRAM Millimeter Summer School 2*, ed. A. Dutrey, 71

¹ Using our $C^{17}(1-0)$, $C^{18}(1-0)$ and $C^{18}(2-1)$ data, we estimate the $C^{18}(2-1)$ optical depth to be 0.7–1 toward IRAM 04191.